




RESEARCH ARTICLE

ORF8 protein of SARS-CoV-2 reduces male fertility in mice

Ting Yu¹ | Qiao Ling¹ | Mengxin Xu² | Niu Wang¹ | Lixia Wang¹ |
Hanwen Lin¹ | Manqi Cao¹ | Yong Ma² | Yuanyuan Wang² | Kuibiao Li³ |
Liubing Du¹ | Yunyun Jin¹ | Ying Li¹ | Deyin Guo¹  | Xiaoxue Peng¹  |
Yao-qing Chen^{2,4} | Bo Zhao¹ | Ji-An Pan¹ 

¹The Center for Infection and Immunity Study and Molecular Cancer Research Center, School of Medicine, Sun Yat-sen University, Shenzhen, Guangdong, China

²School of Public Health (Shenzhen), Sun Yat-sen University, Shenzhen, Guangdong, China

³Guangzhou Center for Diseases Control and Prevention, Guangzhou, Guangdong, China

⁴Key Laboratory of Tropical Disease Control, Ministry of Education, Sun Yat-sen University, Guangzhou, China

Correspondence

Xiaoxue Peng, Ji-An Pan, and Bo Zhao, The Center for Infection and Immunity Study and Molecular Cancer Research Center, School of Medicine, Sun Yat-sen University, Shenzhen 518107, Guangdong, China.

Email: pengxx9@mail.sysu.edu.cn, panjan@mail.sysu.edu.cn, and zhaob39@mail.sysu.edu.cn

Chen Yao-qing, School of Public Health (Shenzhen), Sun Yat-sen University, No. 66, Gongchang Rd, Guangdong, Shenzhen 518107, China.

Email: chenyaoqing@mail.sysu.edu.cn

Funding information

Shenzhen Science and Technology Innovation Program; Natural Science Foundation of Guangdong Province; National Natural Science Foundation of China

Abstract

As one of the most rapidly evolving proteins of the genus *Betacoronavirus*, open reading frames (ORF8's) function and potential pathological consequence in vivo are still obscure. In this study, we show that the secretion of ORF8 is dependent on its N-terminal signal peptide sequence and can be inhibited by reactive oxygen species scavenger and endoplasmic reticulum-Golgi transportation inhibitor in cultured cells. To trace the effect of its possible in vivo secretion, we examined the plasma samples of coronavirus disease 2019 (COVID-19) convalescent patients and found that the patients aged from 40 to 60 had higher antibody titers than those under 40. To explore ORF8's in vivo function, we administered the mice with ORF8 via tail-vein injection to simulate the circulating ORF8 in the patient. Although no apparent difference in body weight, food intake, and vitality was detected between vehicle- and ORF8-treated mice, the latter displayed morphological abnormalities of testes and epididymides, as indicated by the loss of the central ductal lumen accompanied by a decreased fertility in 5-week-old male mice. Furthermore, the analysis of gene expression in the testes between vehicle- and ORF8-treated mice identified a decreased expression of *Col1a1*, the loss of which is known to be associated with mice's infertility. Although whether our observation in mice could be translated to humans remains unclear, our study provides a potential mouse model that can be used to investigate the impact of severe acute respiratory syndrome coronavirus 2 (SARS-CoV-2) infection on the human reproductive system.

KEYWORDS

infertility, ORF8, SARS-CoV-2, secretion

1 | INTRODUCTION

Severe acute respiratory syndrome coronavirus 2 (SARS-CoV-2) has caused one of the most severe pandemics in human history (WHO). Sharing 79.6% sequence identity to SARS-CoV, SARS-CoV-2 causes similar syndromes to (although less severe than)

SARS-CoV. The typical syndromes include fever, dry cough, dyspnea, fatigue, headache, and pneumonia.¹⁻³ Besides these syndromes, the recent studies reported that the infection of SARS-CoV-2 can lead to interstitial edema, congestion, and red blood cell exudation in testes and epididymis, which likely contributes to the reduced sperm count and motility, and even

Ting Yu, Qiao Ling, Mengxin Xu, and Niu Wang contributed equally to this study.

potential infertility.^{4,5} The underlying molecular mechanisms for SARS-CoV-2-specific syndromes are still mostly obscure.

Belonging to the genus *Betacoronavirus* of the Coronaviridae family, SARS-CoV-2 encodes 16 nonstructural proteins (nsps), 4 structural proteins, and at least 7 known accessory proteins using its at least 9 known open reading frames (ORFs). Among all these viral proteins, spike (S) and ORF8 are the most rapidly evolving ones.^{6–12} The rapid evolution of S protein contributes to the different efficiency of viral spread, most likely by increasing its affinity to the host cell receptor, angiotensin-converting enzyme 2 (ACE2), thus promoting the viral entry process. ORF8 of SARS-CoV-2 shares less than 20% sequence identity with its counterpart of SARS-CoV, ORF8a, or ORF8b. Viral sequence analyses have identified frequent mutations or deletions in the ORF8 coding sequence in various strains isolated from patients.^{13–16} However, the advantage of these genetic alternations for the virus is still unknown.

The known function of ORF8 indicates its close relation with immune regulation. ORF8 affects the adaptive immune response and accounts for SARS-CoV-2-mediated downregulation of major histocompatibility complex class I through the lysosome degradation mechanism.¹⁷ ORF8 contributes to cytokine storm by activating the IL-17 pathway.¹⁸ Moreover, ORF8 could affect the innate immune response. The intracellular ORF8 aggregates inhibit IFN- γ -induced antiviral gene expression.¹⁹ It antagonizes the production of interferon- β and alters the interferon regulatory factor 3's binding network, leading to immune evasion.^{20,21}

In this study, we reported that exogenous administration of ORF8 can reduce the fertility of male mice. We showed that the signal peptide at the N-terminus of ORF8 was essential for the secretion of ORF8. The ORF8 was secreted through the canonical endoplasmic reticulum (ER)-Golgi route, which is sensitive to the inhibitory effect of Brefeldin A. The disulfide bonds in the ORF8 render it sensitive to the treatment of Reactive Oxygen Species (ROS) scavengers. ROS scavenger treatment decreased the stability of ORF8 and thus decreased its secretion. By examining the plasma samples from 82 convalescent COVID patients infected with SARS-CoV-2, we found a significant increase in ORF8-specific IgG antibody titers in both female and male patients, indicating a possible *in vivo* secretion of ORF8. To investigate the impact of ORF8 *in vivo*, we administered the ORF8 to the male mice through the tail-vein injection. We observed the swelling testes and epididymides of male mice and a decreased pregnancy rate for female mice, which were mated with ORF8-treated 5-week-old male mice. To delineate the potential target of ORF8, we performed a comparative analysis of gene expression between vehicle and ORF8-treated mice with RNA sequencing (RNA-seq) and identified an expression decrease of *Col1a1*, which is possibly accountable for infertility. We believe this infertility model of male mice may contribute to the research and the development of new therapeutic agents to mitigate or cure SARS-CoV-2-induced infertility.

2 | RESULTS

2.1 | ORF8 is a secretory protein of SARS-CoV-2

ORF8 is one of the most evolving proteins for *Betacoronavirus*, while the knowledge for its *in vivo* function is limited. Using SignalP-5.0, we identified a signal peptide sequence at its N-terminus, indicating that ORF8 may be actively secreted and play an unknown role in the circulation system (Figure 1A).

We first investigated the secretion of ORF8 in mammalian cells. ORF8-green fluorescent protein (GFP) and GFP plasmids were transfected into HEK293T cells. The expression level of ORF8-GFP and GFP in the cell culture medium at multiple time points posttransfection was identified via western blot analysis (WB) (Figure 1B). The results showed that the secretion of ORF8-GFP protein peaked 1 day posttransfection and steadily declined, while on the contrary, the level of GFP protein in the cell culture medium increased gradually, which is likely released by the increased number of dead cells (Figure 1B).

To determine the essential role of signal peptide sequence for the secretion of ORF8, we expressed ORF8-GFP without the signal peptide sequence (Δ 1-14) in the HEK293T cells. We observed that the deletion of the signal peptide sequence decreased both the secreted ORF8 and the intracellular ORF8, indicating that the deletion of signal peptide decreases both the stability (Figure 1C,D) and the secretion (Figure 1C,E) of ORF8.

Disulfide bonds play essential roles in the formation of ORF8 structure.⁸ We treated the cells expressing ORF8 with ROS scavenger, 2,2,6,6-tetramethyl-4-piperidinyl-1-oxy (TEMPO), to disturb the disulfide bond formation of ORF8. The results showed that TEMPO decreased the intracellular protein expression level (Figure 1F,G) and the secretion rate (Figure 1F,H) of ORF8. Seven cysteines in ORF8 are involved in the disulfide bond formation. C25/C90, C37/C102, and C61/C83 form the intramolecular disulfide bonds, whereas C20 is responsible for forming intermolecular disulfide bonds, which are essential for the dimerization of ORF8 (Figure 1A). To dissect the role of each cysteine residue in the secretion of ORF8, we mutagenized each cysteine to serine to disrupt the formation of the related disulfide bond. The mutations of cysteine to serine varied in the alteration of the expression of ORF8 (Figure 1I,J), while most mutations decreased the secretion rate of ORF8 except C20S (Figure 1I,K).

The structure and sequence analysis identified a glycosylation site, N78, in ORF8 (Figure 1A). To determine the role of glycosylation of ORF8 in the secretion, we mutagenized the residue 78 from N to Q, which largely retains the structure and charge of asparagine and thus minimizes the impact of the mutation on the protein folding. N78Q mutation drastically increased the stability and the secretion of ORF8 (Figure 1L,M) and barely altered the secretion rate (Figure 1L,N), indicating that the glycosylation on N78 of ORF8 is not essential for the secretion but plays a crucial role in the degradation of ORF8 protein.

To further determine that the secretion route of ORF8 is from ER to Golgi complex (Golgi), we employed Brefeldin A, an inhibitor preventing the association of COP-1 coat to the Golgi membrane, to treat the cells with the ORF8 expression. The results showed that the treatment of Brefeldin A decreased the secretion of ORF8 (Figure 1O,Q) and led to the accumulation of intracellular ORF8 (Figure 1O,P). We observed that the treatment of Brefeldin A also decreased the secretion of ORF8 with N78Q mutation (Figure 1O,Q). Interestingly, the treatment of Brefeldin A failed to lead to the accumulation of ORF8 with N78Q mutation as it did on wild-type (WT) ORF8 (Figure 1O,P). Our results indicate that together with Golgi, the glycosylation plays a crucial role in ORF8 degradation.

2.2 | Anti-ORF8-specific IgG antibodies were detected in convalescent COVID-19 patients

As discussed in the previous section, we found that ORF8 was secreted in the cell culture system. Next, we sought to investigate whether ORF8 could be secreted in vivo. We measured the antibodies against ORF8 in the serum samples from convalescent COVID-19 patients via enzyme-linked immunosorbent assay (ELISA). Eighty-two COVID-19 convalescent patients were recruited for study at least 14 days after being free of COVID symptoms. The results showed that SARS-CoV-2 infection-induced strong ORF8-specific humoral response in both males and females (Figure 2A,B). Besides, the area value enclosed by the serum

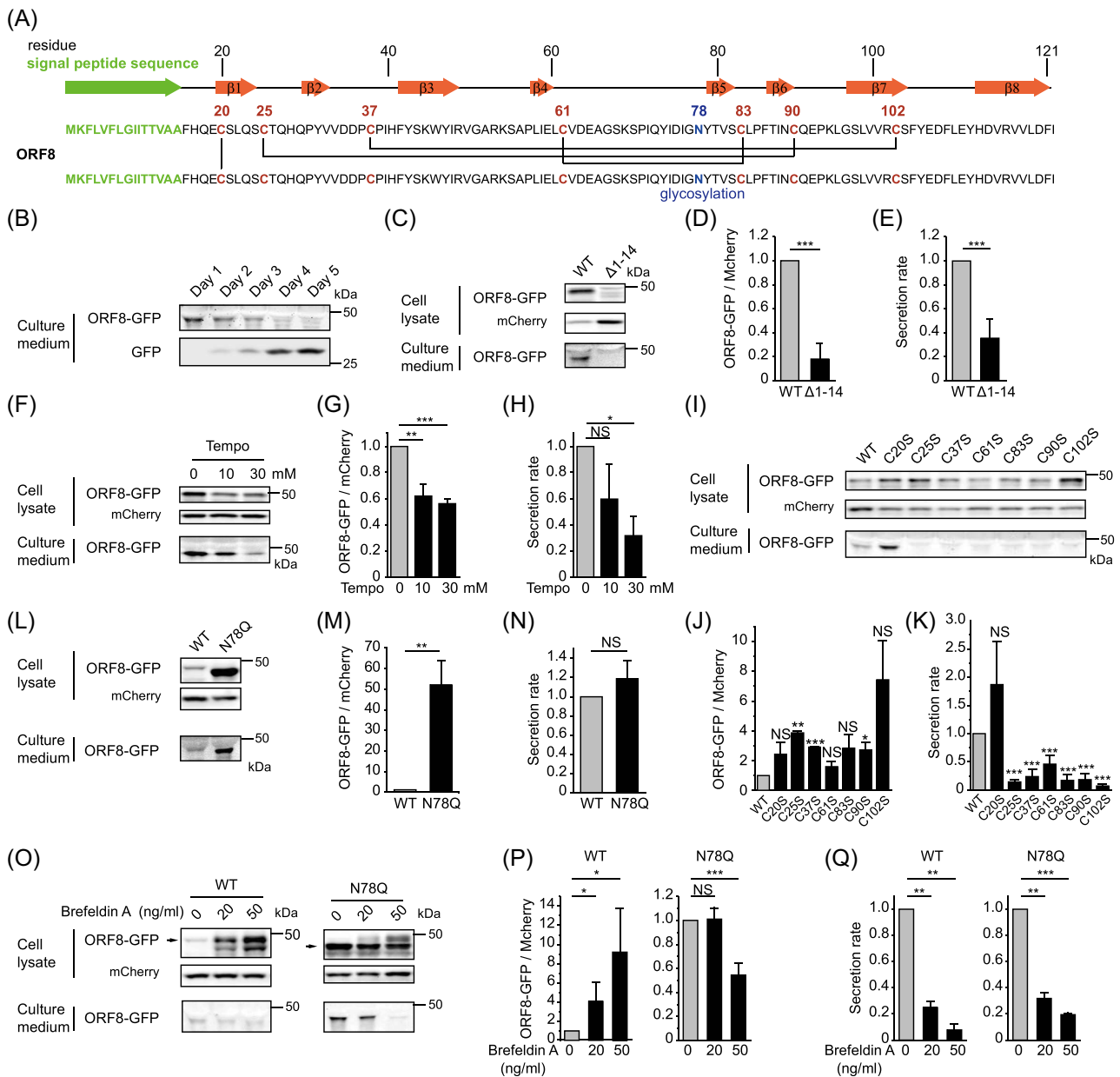


FIGURE 1 (See caption on next page)

dilution curve and the horizontal axis was calculated to determine the area value under the curve. Similarly, both female and male convalescent patients showed higher ORF8-specific IgG antibody titers compared to healthy donors' serum ($p < 0.001$), and no statistical differences were identified between female and male patients (Figure 2C). In addition, we found that the convalescent patients aged between 40 and 60 had higher antibody titers against ORF8 than those under 40 ($p < 0.05$) (Figure 2D). Consistent with the previous report indicating that nucleocapsid, ORF8, and ORF3b proteins elicited the strongest specific antibody response²² in the COVID-19 patients, our results showed a strong ORF8 antibody response retained in COVID-19 convalescent patients and suggested a possible secretion of ORF8 *in vivo*.

Since many serum samples from COVID convalescent patients, which exhibited a strong antibody response to ORF8, were collected at least 14 days after free of symptoms of COVID-19, we speculated the existence of memory B cells expressing ORF8-specific monoclonal antibodies (mAbs) in the blood samples. To enrich these memory B cells, we utilized biotinylated ORF8 as the bait to recognize and sort the specific memory B cells. Variable regions of IgG antibodies were then amplified through single-cell polymerase chain reaction (PCR). After mAbs were cloned into IgG expression vector and purified, three mAbs, CD408, CD513, and CD577, were confirmed to detect ORF8s strongly (Figure 2E).

2.3 | The circulating ORF8 in 5-week-old mice leads to impaired reproductive system

To further investigate the *in vivo* impact of ORF8, we administered ORF8, which was purified via mammalian expression system, to male mice via tail-vein injection. Without knowing the influence of age on the animal sensitivity to the ORF8, we selected 5-week-old and 7-week-old WT C57BL/6 mice.

The administration of ORF8 on mice was performed as described in Figure 3A. We did not observe the noticeable differences in body weight, food intake, and vitality between mice treated with vehicle and ORF8. One week after the last injection, we euthanized the mice and examined the morphological change of various organs. The most apparent difference happened in testes and epididymides. We observed different degrees of swellings on testes (Figure 3B) and epididymides (Figure 3C) of 5-week-old mice, which did not occur on 7-week-old mice.

Due to this phenotype, we speculated about a malfunction of the reproductive system. We first examined the quality of sperm. Morphological differences of sperms between vehicle- and ORF8-treated mice were not evident (Figure 3D). However, a significant increase was observed in the sperm immobility of ORF8-treated 5-week-old mice (Figure 3E), not 7-week-old mice (Figure 3F). To obtain a close look at the reproductive system, we did a histological analysis of testes and epididymides of the mice treated with vehicle or ORF8. The testis histological results showed an apparent injury to the architecture of the seminiferous tubules, as indicated by the partial loss of the central ductal lumen (Figure 3G). Morphological abnormalities of epididymides were also observed, as indicated by the partial loss of inter-luminal tissue (Figure 3H). Consistent with data of sperm immobility (Figure 3E,F), more pathological lesions were observed in the ORF8-treated 5-week-old mice than ORF8-treated 7-week-old mice (Figure 3I,J), indicating that 5-week-old mice are more vulnerable to the treatment of ORF8 than 7-week-old mice.

2.4 | The circulating ORF8 induced the infertility of 5-week-old male mice

To investigate the functional consequences of the circulating ORF8 on the reproductive system, we first examined testosterone levels in the blood. We cannot detect a statistically significant difference in

FIGURE 1 ORF8 is a secretory protein of SARS-CoV-2. (A) Schematic illustration of the structure of ORF8. ORF8 protein has a 14-aa signal peptide sequence (green arrow and letters in green) and eight beta-strands (orange arrows). Seven cysteine residues (red) are involved in the disulfide bond formation. The pairs of cysteine residues, which form the disulfide bonds, are linked with lines. The cysteine residue 20 mediated the intermolecular disulfide bond formation. (B) HEK293T cells were transfected with the ORF8-GFP and GFP plasmids. One day posttransfection, the supernatants were collected and replaced with a fresh medium. The supernatants were subjected to WB and detected with a GFP antibody. (C) HEK293T cells were transfected with the ORF8-GFP WT or $\Delta 1-14$ mutant and mCherry plasmids. One day posttransfection, the supernatants were collected, and the cells were lysed in RIPA buffer containing 1% SDS. The samples were subjected to WB analysis. The densitometry of each band was performed with Image Studio™ Lite software. (D) The relative expression levels of WT and $\Delta 1-14$ were obtained by normalizing with the amount of WT and $\Delta 1-14$ with that of mCherry. (E) The secretion rate of WT or $\Delta 1-14$ was obtained by normalizing the WT or $\Delta 1-14$ amount of the culture medium with that of cell lysate. HEK293T cells were transfected with the ORF8-GFP WT and mCherry plasmids and then treated with TEMPO at indicated concentrations. (F) The samples were subjected to WB analysis. The relative expression and the secretion rate of ORF8-GFP were presented in (G) and (H), respectively. Same as (C–E), the samples for ORF8-GFP WT or various cysteine mutants were examined with WB (I), and the relative expression and the secretion rate of ORF8-GFP were presented in (J) and (K), respectively. Like (C–E), the samples for ORF8-GFP WT or N78Q mutant were examined with WB (L). The relative expression (M) and the secretion rate (N) of ORF8-GFP or N78Q were presented. HEK293T cells were transfected with ORF8-GFP or N78Q mutant and then treated with Brefeldin A at indicated concentrations. The samples were subjected to WB (O), the relative expression and the secretion rate of ORF8-GFP or N78Q were presented in (P) and (Q), respectively. Data are presented as mean \pm SEM; * $p < 0.05$, ** $p < 0.01$, *** $p < 0.001$; two-tailed unpaired Student's *t*-test. GFP, green fluorescent protein; ORF, open reading frames; RIPA, radioimmunoprecipitation assay; SARS-CoV-2, severe acute respiratory syndrome coronavirus 2; SDS, sodium dodecyl sulfate; SEM, standard error of mean; TEMPO, 2,2,6,6-tetramethyl-4-piperidinyl-1-oxyl; WB, western blot analysis; WT, wild-type.

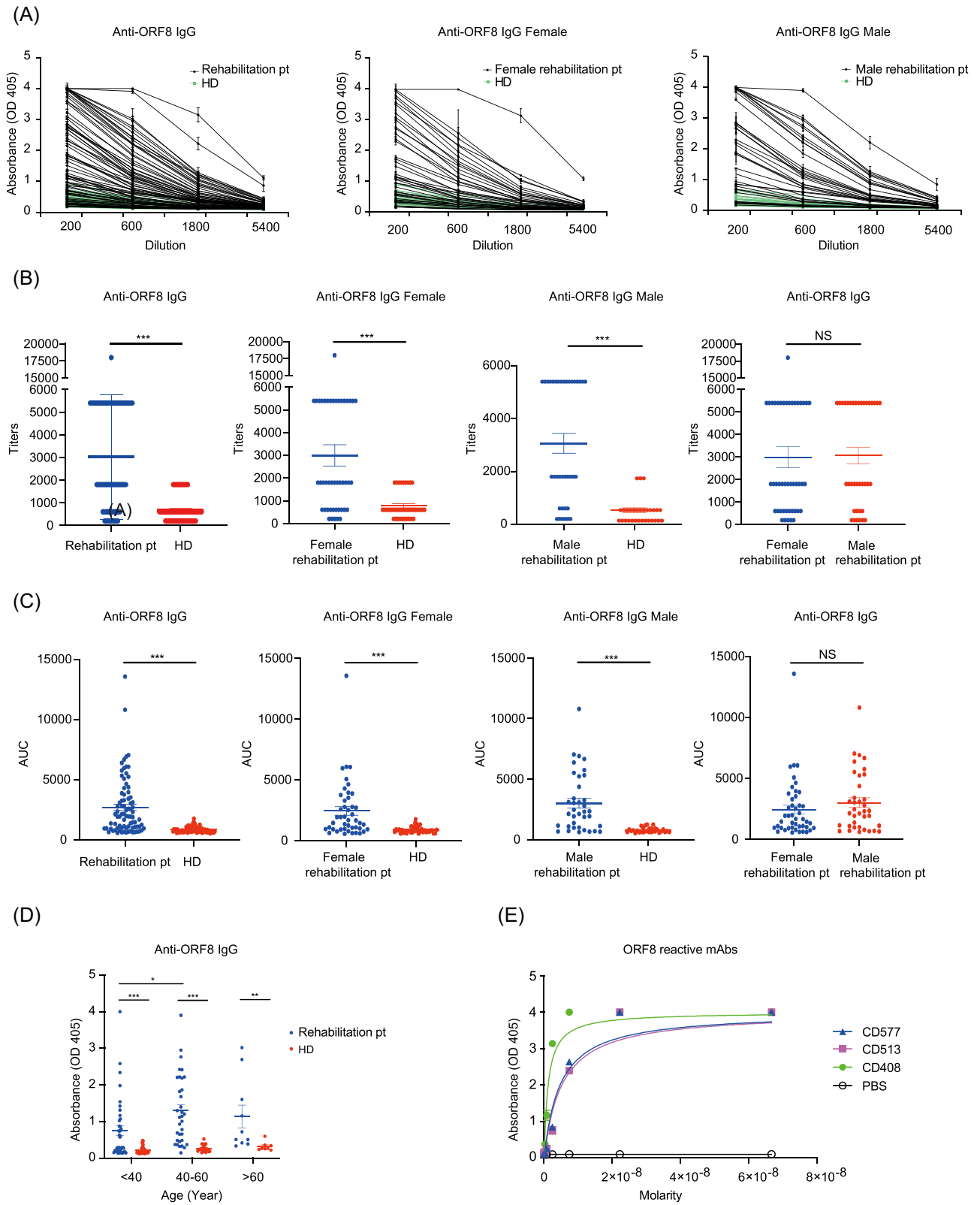


FIGURE 2 (See caption on next page)

the blood testosterone level between vehicle- and ORF8-treated mice, consistent with the aforementioned data of no evident morphological differences of sperms between vehicle- and ORF8-treated mice (Figures 3D and 4A).

Next, we mated the female mice with vehicle- or ORF8-treated male mice. Consistent with the substantial injury to testes and epididymides, the pregnancy rate was reduced significantly for female mice mated with ORF8-treated 5-week-old male mice (9 nonpregnant out of total 14) compared with vehicle-treated 5-week-old male mice (1 nonpregnant out of total 10), as indicated by the difference in body weight increase and the delivery of live fetuses (Figure 4B,D). A similar difference was not observed for the 7-week-old male mice (Figure 4C,E). No significant difference in the number of live fetuses recovered from pregnant females was observed, while 3 out of 14 female mice, all of which mated with ORF8-treated 5-week-old male mice, gained weight in the early days after mating, failed to retain the body weight increase, and failed to give the normal fetuses. Moreover, we observed an apparent delay in the delivery of female mice mated with ORF8-treated 5-week-old male mice, suggesting that ORF8 treatment could affect male fertility by possibly reducing the sex drive (Figure 4B).

To further explore the molecular mechanism for ORF8-induced infertility, we analyzed the gene expressions in the homogenate of testes via RNA-seq. The RNA-seq results identified 80 upregulated genes (Figure 4F,G) and 126 downregulated genes (Figure 4F,H and Supporting Information: Table 1). Although a set of DNA-binding transcription factors and activators for RNA polymerase II was decreased by ORF8 treatment (Figure 4H), drastic increases in the amount of the proteins functioning in integrin binding and protein binding were identified, indicating a possible elevated activity for an injury-driven tissue repair (Figure 4G). Moreover, Col11a2 and Col1a1 functioning in extracellular matrix structural conferring tensile strength were downregulated (Figure 4F). Silencing of Col1a1 was shown to suppress spermatogonia self-renewal.²³ Thus, Col1a1 could be a breakthrough point in investigating the mechanism of ORF8-caused the infertility of male mice.

3 | DISCUSSION

Consistent with a previous report,¹⁷ we confirmed that the signal peptide at the N-terminus regulated the secretion of ORF8, leading us to explore a possible extracellular function of ORF8. Our study

confirmed the crucial roles of disulfide bonds in stabilizing the ORF8 structure by altering the redox homeostasis or mutagenizing the cysteines in ORF8, indicating antioxidants' therapeutic potential in the treatment of ORF8-associated symptoms. Moreover, our evidence suggested that ORF8 was degraded in glycosylation and Golgi-dependent manner, indicating that the Endosome and Golgi-associated degradation plays a crucial role in the protein turnover of ORF8.

Hachim et al. reported that nucleocapsid, ORF8, and ORF3b proteins elicited the strongest specific antibody response in COVID-19 patients. Similarly, our results showed that a strong ORF8 antibody response was retained in COVID-19 convalescent patients, and the antibody response had no gender preference. Our study first identified that ORF8 elicited a more robust antibody response in convalescent patients aged from 40 to 60 than those under 40. Together with the data from cell culture, these data indicated a possible function of ORF8 in the circulation system.

To determine the impact of ORF8 in vivo, we employed purified ORF8 protein to treat male mice through tail-vein injection. Histological results showed the loss of germ cells and sloughing of luminal cells from testicular tubular basement membranes, which is consistent with the previous observation on the tissues from deceased COVID patients.²⁴

Viral infections lead to male infertility, either by directly attacking the reproductive system or indirectly by eliciting the local immunological or inflammatory responses to damage the reproductive system.²⁵ Various viruses, including Zika,²⁶ Mumps,²⁷ HBV,²⁸ HPV,²⁹ HSV,³⁰ and HCV,³¹ are known to cause male infertility. The SARS-CoV-2 infection has been reported to impair sperm quality³² and causes significant seminiferous tubular injury, reduced Leydig cells, and mild lymphocytic inflammation.²⁴ In the last several months, we witnessed a rapidly growing body of literature concerning SARS-CoV-2-related infertility, but the clue for the mechanistic explanation is still limited. Most attention has focused on a possible direct infection of SARS-CoV-2, largely because the elevated expression of ACE2 has been found in testicular Sertoli cells, Leydig cells, and glandular cells of the seminal vesicle, as compared with other tissues.^{33,34} However, several independent studies showed no evidence of SARS-CoV-2 in semen.³⁵⁻³⁷ Since the phenotype in our study was induced by ORF8, and mouse ACE2 cannot function as the cell-entry receptor for SARS-CoV-2, we speculate that instead of direct viral invasion, SARS-CoV-2 can indirectly impair male fertility.

FIGURE 2 Anti-ORF8-specific IgG antibodies were detected in convalescent COVID-19 patients. (A) Serial dilutions of plasma samples were analyzed for binding to ORF8 via ELISA. The initial dilutions for plasma in COVID-19 convalescent patients ($n = 82$) and healthy donors ($n = 69$) were 1:200, followed by a threefold serial dilution. (B) Anti SARS-CoV-2 ORF8 antibody titers in COVID-19 convalescent patients and healthy donors determined by ELISA. (C) Data from the same experiments with (A) were presented as AUC. (D) IgG response against ORF8 in different age groups of COVID-19 convalescent patients. (E) Three ORF8 specific antibodies were cloned from the memory B cells from COVID-19 convalescent patient, and the titers of antibodies were examined as presented. AUC, area under curve; COVID, coronavirus; ELISA, enzyme-linked immunosorbent assay; HD, healthy donor; NS, not significant; ORF, open reading frames; Pt, patient; SARS-CoV-2, severe acute respiratory syndrome coronavirus 2. Data are representative of two independent experiments. Data are presented as mean \pm SEM. Comparisons between two groups were performed using a nonparametric rank-sum test. $p < 0.05$ were considered significant. * $p < 0.05$, ** $p < 0.01$, *** $p < 0.001$.

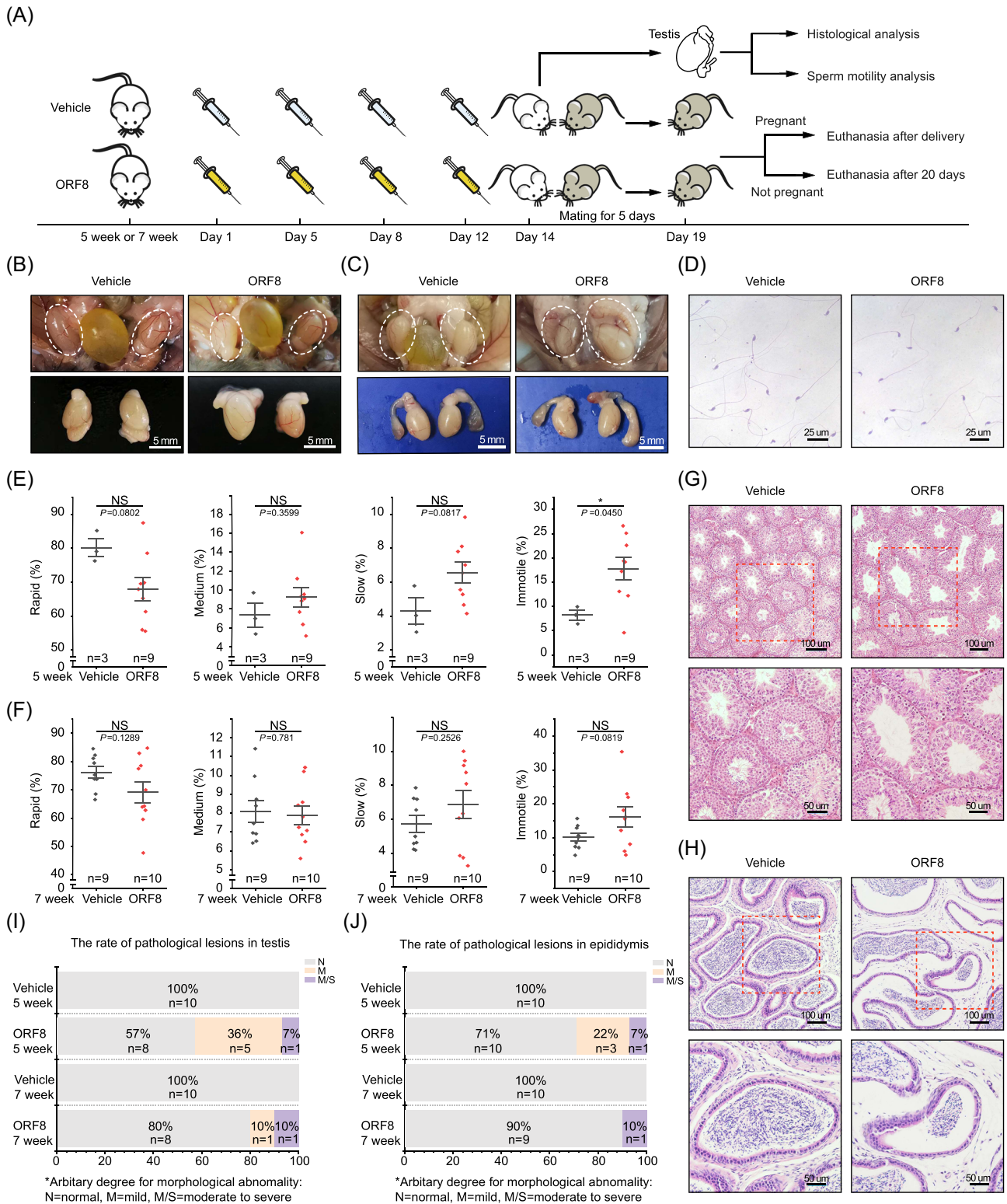


FIGURE 3 The circulating ORF8 in 5-week-old mice leads to the impaired reproductive tract. (A) Experimental design schematic for the administration of ORF8 on male mice and the mating. The image of in situ or isolated swelling testes (B) and epididymides (C). (D) The image of sperms from vehicle- or ORF8-treated 5-week-old mice. Computer-assisted sperm analysis on the portions of sperms with different motility rates from 5-week-old (E) and 7-week-old mice (F). Histological analysis of testes (G) and epididymides (H) collected from vehicle- or ORF8-treated mice stained with haematoxylin and eosin. The analysis of the pathological lesions in testes (I) and epididymides (J). According to the severity, the injury was arbitrarily categorized into three classes, normal, mild, and moderate to severe. Data are presented as mean ± SEM; **p* < 0.05, ***p* < 0.01, ****p* < 0.001; two-tailed unpaired Student's *t*-test. ORF, open reading frames.

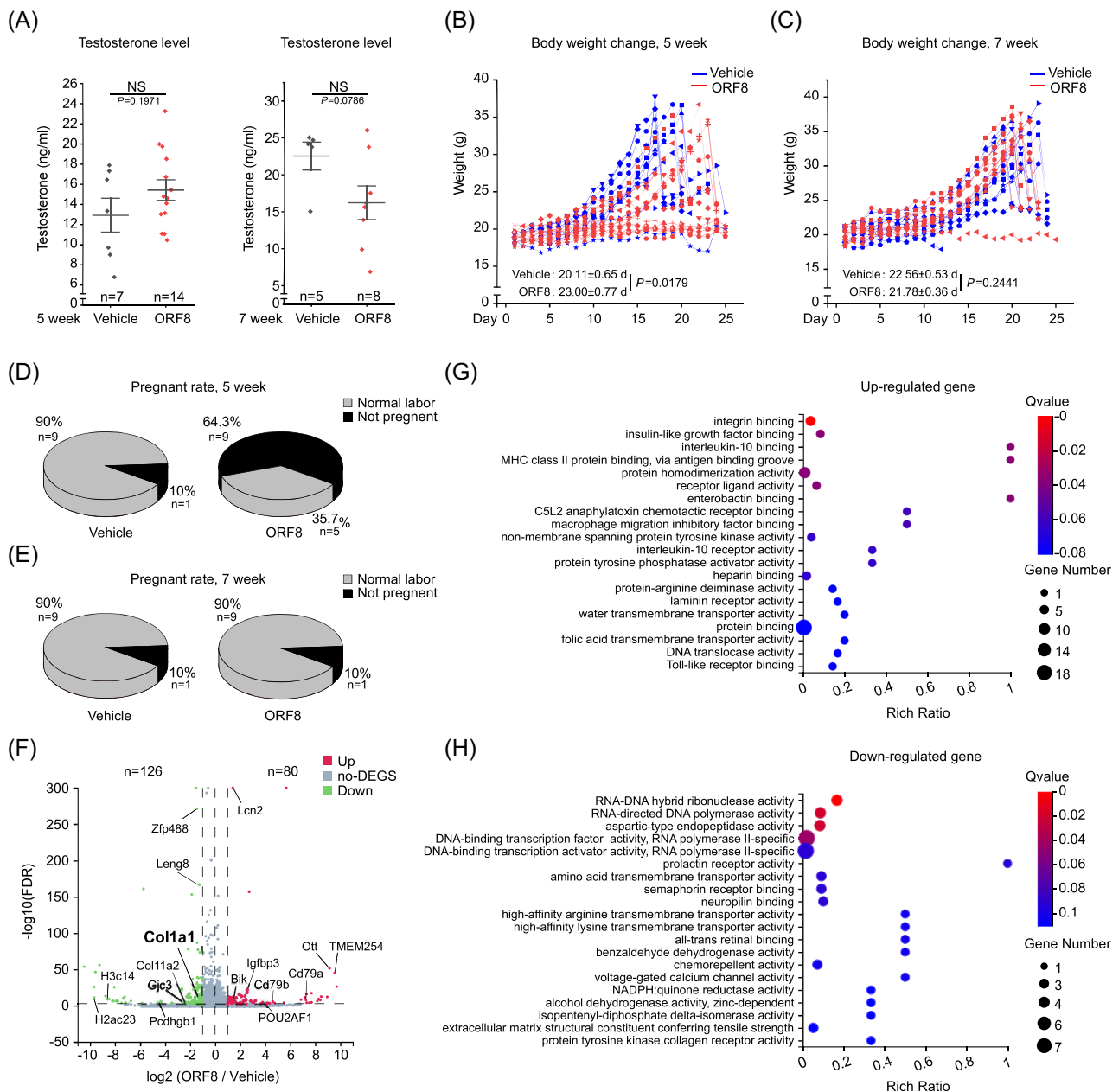


FIGURE 4 The circulating ORF8 induced the infertility of 5-week-old male mice. (A) The testosterone level of vehicle- and ORF8-treated male mice. The body weight (B and C) and the pregnancy rate (D and E) of female mice after being mated with male mice. The RNA of testis homogenates were subjected to RNA-seq analysis. The distribution and false discovery rate of various genes were presented in (F). The upregulated genes (G) and downregulated genes (H) were categorized according to their known main function. Data are presented as mean \pm SEM; * $p < 0.05$, ** $p < 0.01$, *** $p < 0.001$; two-tailed unpaired Student's *t*-test. ORF, open reading frames; RNA seq, RNA sequencing.

Genome-wide RNA-seq analysis identified a drastic decrease in the messenger RNA (mRNA) level of Col1a1 in the testes of ORF8-treated mice. Col1a1 is one of the major subunits of type I collagen, the major component of connective tissue, providing the connection between Sertoli cells and germ cells. Thus, Col1a1 plays an essential role in maintaining spermatogonial homeostasis.^{23,38} Our study showed that 5-week-old mice were more sensitive to the ORF8 treatment than 7-week-old mice. Interestingly, Col1a1 expression in 6-day-old mice was at a much higher

level than in 60-day-old mice, indicating a possible correlation between the expression level of Col1a1 and sensitivity to ORF8-induced infertility.²³ The mechanistic explanation for the association between ORF8 and Col1a1 awaits further investigations.

We acknowledge that the results in this study may only reflect the impact of ORF8 in mice. At the same time, considering the similar infertility phenotype between humans and mice, including the similar injury in the ductal lumen in the reproductive system, we believe this infertility model of male mice may benefit

the research and the development of new therapeutic agents to mitigate or cure SARS-CoV-2-induced infertility. Our study also raises a concern about the safety of the attenuated SARS-CoV-2 vaccine under development, which retains the ability to express ORF8.

4 | MATERIALS AND METHODS

4.1 | Cell lines and culture

HEK293T, U-2 OS, and Vero E6 cell lines are cultured in Dulbecco's modified Eagle's medium (DMEM) (Thermo Fisher Scientific; C11960500), supplemented with 10% fetal bovine serum (PAN Biotech; ST30-3302), 100 unit/ml penicillin, 100 µg/ml streptomycin (Thermo Fisher Scientific; 15140-122), which is designated as a complete medium, at 37°C with 5% CO₂.

4.2 | Plasmid construction

The coding sequences of ORF8 were amplified from COVID-19 replicons,³⁹ based on the strain of SARS-CoV-2 Wuhan-Hu-1 (MN908947.3) with PCR. The PCR fragment was inserted into LPC vector,⁴⁰ with a tandem tag of HA/FLAG and His after the insertion site for ORF8. We failed to obtain a decent expression of both ORF8-HA-His and ORF8-FLAG-His. In our lab practice, we fuse the protein with GFP to improve its expression.¹⁰ Accordingly, we constructed the plasmid, which expresses ORF8-GFP in the mammalian cells. Δ1-14 ORF8-GFP was constructed by replacing the WT ORF8 with ORF8 with the deletion of aa 1-14 (KFLVFLGIITVAA). The glycosylation mutation of N78Q and the cysteine mutations of C20S, C25S, C37S, C61S, C83S, C90S, and C102S were performed using site-directed mutagenesis procedure as described previously.⁴¹

4.3 | Protein expression and purification

A PCR fragment encoding WT ORF8 was cloned into the pcDNA3.4 mammalian expression vector. The construct contains an N-terminal 10xHis tag followed by a Strep-Tag II sequence and a 3C protease site. ORF8 recombinant protein was expressed using Expi293F cells in suspension culture with OPM CD05 serum-free medium (OPM Biosciences; 81075-001). Supernatant was harvested after 5 days and purified using Ni-NTA affinity column (Qiagen) followed by StrepTrap HP column (Cytiva). ORF8 was cleaved with 3C protease at 4°C overnight and further purified by gel filtration (Superdex 200; Cytiva). Purified ORF8 was dialyzed in PBS buffer (pH 7.4) and then sterilized by being passed through a 0.22 µm filter. The final protein of 1 mg/ml in sterile PBS buffer was used for mouse injection.

4.4 | Transfections

HEK293T, U-2 OS, or Vero E6 were transfected with LPC-ORF8-GFP and mCherry plasmids using Hieff Trans™ Liposomal Transfection Reagent (Yeasen Biotech; 40802ES03) following the manufacturer's instructions. Briefly, 1 day before transfection, 1.5×10^6 cells were plated in a 6 cm dish. One hour before transfection, the complete medium was replaced with DMEM. The mixture of plasmids and Liposomal Transfection Reagent was dropwise added in the cell culture. Seven hours posttransfection, the culture medium was replaced with a complete fresh medium and then treated with indicated drugs. The culture medium was collected for the detection of secretory proteins, and the same volume of complete fresh medium was added into the dishes at indicated time points.

4.5 | Reagents and antibodies

The following antibodies were used: polyclonal rabbit anti-GFP antibody (Proteintech; 50430-2-AP; 1:1000 for WB), mouse anti-mCherry antibody (Abbkine; A02080; 1:1000 for WB), goat anti-mouse antibody (LI-COR; 926-32211; 1:10 000 for WB), goat anti-rabbit antibody (LI-COR; 926-68070; 1:10 000 for WB), Alexa Fluor™ 594 goat anti-mouse IgG (H + L) (Thermo Fisher Scientific; A11005, 1:1000 for IF), and Alexa Fluor™ 488 goat anti-rabbit IgG (H + L) (Thermo Fisher Scientific; A11008; 1:1000 for IF).

The following reagents were used: TEMPO (Sigma-Aldrich; 214000), Brefeldin A (Topscience; T6062), TRIZOL™ Reagent (Invitrogen; AM9738), propidium iodide (Yeason; 25535-16-4), SYBR Premix Ex Taq (TA-KARA; RR420A), and Revert Aid First Strand cDNA Synthesis Kit (Thermo Fisher Scientific; K1622), Hieff Trans™ Liposomal Transfection Reagent (Yeasen; 40802 ES03), Pierce™ BCA Protein Assay Kit (Thermo Fisher Scientific; 23227), paraffin (Thermo Fisher Scientific; 8330), xylene (Sangon Biotech; A530011-0500), Hematoxylin-Eosin (HE) staining kit (Sangon Biotech; E607318-0200), Ready To Use HP IHC Detection Kit (Absin; abs957), T (Testosterone) ELISA Kit (Sangon Biotech; D751045-0096).

4.6 | WB

HEK293T and Vero E6 cells from different dishes were lysed in the same volume of RIPA buffer (50 mM Tris-HCl, pH 8.0, 0.5% sodium deoxycholate, 1% sodium dodecyl sulfate (SDS), 1% Triton-X-100, 150 mM NaCl). All lysates were quantified using BCA protein assay reagent (Thermo Fisher Scientific; 23227) and loaded into the 12.5% sodium dodecyl sulfate-polyacrylamide gel electrophoresis (SDS-PAGE). The cell culture supernatants from different dishes were collected, and the volumes of different samples for SDS-PAGE analysis were determined according to the loading volumes of the related cell lysates. After SDS-PAGE, the samples in the gel were transferred to nitrocellulose membranes. After being blocked with

blocking buffer (PBS containing 5% nonfat milk and 0.05% Tween 20 (PBST) for 1 h at room temperature, the membrane was incubated in blocking buffer containing primary antibodies (1:1000) against GFP and mCherry overnight at 4°C. After being washed five times with PBST, the membrane was incubated in blocking buffer containing the goat anti-rabbit or goat anti-mouse secondary antibody (1:10 000) for 1 h at room temperature. After being washed five times with PBST, the membrane was imaged and analyzed with an Odyssey Imager (LI-COR), and all the bands were normalized with mCherry bands, which served as the internal reference.

4.7 | Patient samples

A total of 82 COVID-19 convalescent patients' blood samples were enrolled for study during the early stages of the outbreak from February 2020 to March 2020, at least 14 days after being free of symptoms of COVID-19. Of these convalescent patients, 45 (54.88%) were female, and 37 (45.12%) were male. Sixty-nine healthy donors were acquired as negative control before the pandemic outbreak. All study procedures were approved by the Research Ethics Committee of School of Public Health (Shenzhen), Sun Yat-sen University, China.

4.8 | ELISA

Ninety-six-well high-protein binding microtiter plates (Costar) were coated with 50 µl of SARS-CoV-2 ORF8 at 2 µg/ml in PBS and incubated overnight at 4°C. After washing the plates six times with PBS containing 0.2% Tween 20 and blocking with PBS containing 3% BSA, threefold serially diluted mAbs starting at 10 µg/ml (or 1:200 COVID-19 convalescent plasma) were added into the plates and incubated for 1 h at 37°C. Plates were washed six times with PBST and then incubated with HRP (horseradish peroxidase)-conjugated goat anti-human IgG (JACKON) for 1 h at 37°C. The plate was developed with Super Aquablue ELISA substrate (eBiosciences). Absorbance was measured at 405 nm for 10 min at 25°C on a microplate spectrophotometer (BioTek). The data were analyzed using GraphPad Prism (version 8).

4.9 | Flow cytometry

Peripheral blood mononuclear cells in blood samples from COVID-19 convalescent patients were extracted using a human lymphocyte separation medium and then stained with the following fluorescent antibodies: CD19-PB, CD27-APC, and CD38-PE (Biolegend). ORF8 was biotinylated using the NHS-PEG4-BIOTIN (Invitrogen) and then conjugated with FITC-streptavidin (Biolegend), according to the manufacturer's instructions. Flow cytometry analysis was mainly performed as previously described.⁴² Specifically labeled cells were sorted by FACS with a MoFlo Astrios EQ Flow Cytometer (Beckman).

4.10 | mAbs expression and purification

Variable regions of IgG antibodies were amplified through single-cell PCR, and then mAb coding sequences were cloned into IgG expression vector containing the human IgG constant regions. IgG mAbs were expressed by transfecting HEK293T cells with equal amounts of heavy- and light-chain plasmids using polyethylenimine and cultured for 5 days. The supernatant was collected and purified using protein A agarose beads.⁹

4.11 | Mouse ORF8-treated experiments

Five-week and 7-week-old C57BL/6 male and female mice were purchased from the Guangdong medical laboratory animal center and housed under specific-pathogen-free condition. The protocols involving animals were approved by the Animal Ethics Committee of Sun Yat-sen University. The males of the same age were randomly divided into vehicle-treated group and ORF8-treated group, and were administered with vehicle and purified ORF8 (2 µg protein per gram of body weight) via the tail-vein injection four times within 2 weeks. The protein was diluted in Tris-NaCl buffer (20 mM Tris-HCl, pH 8.8, 150 mM NaCl). One week after the last injection, the mice were euthanized, the blood was drawn for the measurement of testosterone, the sperms were collected for computer-assisted sperm analysis (CASA), and the tissues were collected for RNA-seq, H & E staining.

4.12 | Histology

Tissues were harvested after dissection. The testes and epididymides were fixed in Bouin's solution (PythonBio; AAPR437-500) overnight. Five micrometer-thick tissue sections from vehicle- and ORF8-treated mice were processed for histology by H & E staining or immunohistochemistry, and the section was sealed with a neutral resin (Solarbio; G8590). In the H & E staining process, the sections were stained with HE staining kit (Sangon Biotech; E607318-0200).

4.13 | Measurement of testosterone

Eight hundred microliters of mouse blood was mixed with 80 µl 10% sodium citrate solution. The mixture was centrifuged at 500g at 4°C for 10 min, and the supernatant was collected and subjected to testosterone assay by Sangon Biotech.

4.14 | CASA

One week after the last injection, the mice were euthanized, and the sperms from the caudal epididymis of vehicle- and ORF8-treated males were collected immediately after dissection. The sperm

suspension in DMEM/F12 (Thermo Fisher Scientific; 11320033) was analyzed for sperm motility by CASA using the automatic sperm analyzer—MICROPTIC SCA[®] CASA System. All measurements were finished within 10 min after the dissection of cauda epididymis.

4.15 | Fertility studies

One day after the last injection, vehicle and ORF8-treated males were mated with single age-matched female WT C57BL/6 mice. Five days later, male mice were removed from the cage to terminate the mating. The body weight values of each female were recorded daily to monitor the pregnancy. After giving the birth of fetuses, the female mice were euthanized, and the uteruses were collected for histology analysis.

4.16 | Sample preparation for RNA-seq

The vehicle or ORF8-treated testes were chopped into small pieces, and one-fourth of homogenate from one testis was resuspended and incubated in 1 ml TRIzol[™] Reagent for 30 min. The following procedure was performed by following the manufacturer's instructions. RNA purity and concentration were determined using NanoDrop One (Thermo Fisher Scientific) and 1% agarose gel electrophoresis.

4.17 | RNA-seq

RNA-seq was performed by BGI. In brief, mRNAs were purified with Oligo(dT)-attached magnetic beads and fragmented with fragment buffer (BGI). First-strand complementary DNA (cDNA) was generated using reverse transcription with random hexamer primers, followed by second-strand cDNA synthesis. A-Tailing Mix and RNA index adapters were added. The cDNA fragments obtained from the previous step were amplified by PCR, and the products were purified by Ampure XP Beads and then dissolved in elution buffer solution. The product quality was validated on the Agilent Technologies 2100 bioanalyzer, and then the products were heated, denatured, and circularized by the splint oligo sequence to obtain the final library. The single-strand circle DNA (ssCir DNA) was formatted as the final library. The final library was amplified with phi29 DNA polymerase to make DNA nanoball (DNB), which had more than 300 copies of one molecular, DNBS were loaded into the patterned nanoarray, and single-end 50-base reads were generated on BGISEQ500 platform (BGI).

4.18 | RNA-seq informatics analysis

The sequencing data were filtered with SOAPnuke (v1.5.2) by (1) Removing reads containing sequencing adapter; (2) Removing reads

whose low-quality base ratio (base quality less than or equal to five) is more than 20%; (3) Removing reads whose unknown base ("N" base) ratio is more than 5%, afterwards clean reads were obtained and stored in FASTQ format. The clean reads were mapped to the reference genome using HISAT2 (v2.0.4). Bowtie2 (v2.2.5) was applied to align the clean reads to the reference coding gene set, then the expression level of the gene was calculated by RSEM (v1.2.12). The heatmap was drawn by pheatmap (v1.0.8) according to the gene expression in different samples. Essentially, differential expression analysis was performed using the DESeq2 (v1.4.5) with $Q < 0.05$. To take an insight into the change of phenotype, GO (<http://www.geneontology.org/>) and KEGG (<https://www.kegg.jp/>) enrichment analysis of annotated different expressed genes were performed by Phyper based on Hypergeometric test. The significant levels of terms and pathways were corrected by Q value with a rigorous threshold ($Q < 0.05$) by Bonferroni.

4.19 | Statistical analysis

Statistical significance was performed using Origin 8.0 or Prism GraphPad. All the experiments were performed at least three times. Differences between two or three groups were analyzed by Student's t -test or one-way analysis of variance. Results were considered significant when $p < 0.05$.

4.20 | Image processing

Images were processed in Adobe Photoshop and Illustrator. The densitometry of immunoblot bands were determined with Image Studio[™] Lite Software (LI-COR Biosciences).

AUTHOR CONTRIBUTIONS

Ji-An Pan conceived the ideas and designed the experiments. Ji-An Pan, Bo Zhao, Yao-qing Chen, and Xiaoxue Peng wrote the paper. All authors performed experiments or data analysis. All authors read and approved the final manuscript for publication.

ACKNOWLEDGMENTS

We thank Mr. Tong Kuijie and Ms. Jiang Yiling for their technical assistance. This study was supported by grants, Natural Science Foundation of China (#31971161 for Ji-An Pan, #31900546 and #82150204 for Xiaoxue Peng, #31971145 for Bo Zhao, #32041002 for Deyin Guo, #82041046 and #31970881 for Yao-qing Chen, and #32000863 for Ying Li); Natural Science Foundation of Guangdong (2019A1515011332 for Ji-An Pan); and Shenzhen Science and Technology Program (JCYJ20190807160615255 for Ji-An Pan, JCYJ20190807155215221 for Bo Zhao, JSGG20200225150431472 and KQTD20200820145822023 for Deyin Guo, KQTD201804111 43323605 for Yao-qing Chen, and JCYJ20190807153203560 for

Xiaoxue Peng). Deyin Guo is supported by Guangdong Zhujiang Talents Program and National Ten-thousand Talents Program. Bo Zhao is supported by Guangdong Zhujiang Talents Program (2019QN01Y305) and the Guangdong Provincial Key Laboratory of Digestive Cancer Research (2021B1212040006).

CONFLICT OF INTEREST

The authors declare no conflict of interest.

DATA AVAILABILITY STATEMENT

All data generated or analyzed during this study are included in this published article.

ETHICS STATEMENT

The protocols involving animals were approved by the Animal Ethics Committee of Sun Yat-sen University. All study procedures for patient samples were approved by the Research Ethics Committee of School of Public Health (Shenzhen), Sun Yat-sen University. The authors agreed to participate in the project.

ORCID

Deyin Guo  <http://orcid.org/0000-0002-8297-0814>

Xiaoxue Peng  <http://orcid.org/0000-0001-8687-9711>

Ji-An Pan  <http://orcid.org/0000-0002-2842-4126>

REFERENCES

- Jin YH, Cai L, Cheng ZS, et al. A rapid advice guideline for the diagnosis and treatment of 2019 novel coronavirus (2019-nCoV) infected pneumonia (standard version). *Mil Med Res.* 2020;7:4.
- Zhou P, Yang XL, Wang XG, et al. A pneumonia outbreak associated with a new coronavirus of probable bat origin. *Nature.* 2020;579:270-273.
- Wiersinga WJ, Rhodes A, Cheng AC, Peacock SJ, Prescott HC. Pathophysiology, transmission, diagnosis, and treatment of coronavirus disease 2019 (COVID-19): a review. *JAMA.* 2020;324:782-793.
- He Y, Wang J, Ren J, Zhao Y, Chen J, Chen X. Effect of COVID-19 on male reproductive system—a systematic review. *Front Endocrinol (Lausanne).* 2021;12:677701.
- Li H, Xiao X, Zhang J, et al. Impaired spermatogenesis in COVID-19 patients. *EClinicalMedicine.* 2020;28:100604.
- Pereira F. SARS-CoV-2 variants combining spike mutations and the absence of ORF8 may be more transmissible and require close monitoring. *Biochem Biophys Res Commun.* 2021;550:8-14.
- Pereira F. Evolutionary dynamics of the SARS-CoV-2 ORF8 accessory gene. *Infect Genet Evol.* 2020;85:104525.
- Flower TG, Buffalo CZ, Hooy RM, Allaire M, Ren X, Hurley JH. Structure of SARS-CoV-2 ORF8, a rapidly evolving immune evasion protein. *Proc Natl Acad Sci USA.* 2021;118:1-6.
- He B, Liu S, Wang Y, et al. Rapid isolation and immune profiling of SARS-CoV-2 specific memory B cell in convalescent COVID-19 patients via LIBRA-seq. *Signal Transduct Target Ther.* 2021;6:195.
- Jiang Y, Tong K, Yao R, et al. Genome-wide analysis of protein-protein interactions and involvement of viral proteins in SARS-CoV-2 replication. *Cell Biosci.* 2021;11:140.
- Guruprasad L. Human SARS CoV-2 spike protein mutations. *Proteins.* 2021;89:569-576.
- Hussain M, Shabbir S, Amanullah A, Raza F, Imdad MJ, Zahid S. Immunoinformatic analysis of structural and epitope variations in the spike and Orf8 proteins of SARS-CoV-2/B.1.1.7. *J Med Virol.* 2021;93:4461-4468.
- Muth D, Corman VM, Roth H, et al. Attenuation of replication by a 29 nucleotide deletion in SARS-coronavirus acquired during the early stages of human-to-human transmission. *Sci Rep.* 2018;8:15177.
- Gong YN, Tsao KC, Hsiao MJ, et al. SARS-CoV-2 genomic surveillance in Taiwan revealed novel ORF8-deletion mutant and clade possibly associated with infections in Middle East. *Emerg Microbes Infect.* 2020;9:1457-1466.
- Farkas C, Mella A, Turgeon M, Haigh JJ. A novel SARS-CoV-2 viral sequence bioinformatic pipeline has found genetic evidence that the viral 3' untranslated region (UTR) is evolving and generating increased viral diversity. *Front Microbiol.* 2021;12:665041.
- Young BE, Fong SW, Chan YH, et al. Effects of a major deletion in the SARS-CoV-2 genome on the severity of infection and the inflammatory response: an observational cohort study. *Lancet.* 2020;396:603-611.
- Zhang Y, Chen Y, Li Y, et al. The ORF8 protein of SARS-CoV-2 mediates immune evasion through down-regulating MHC-Iota. *Proc Natl Acad Sci USA.* 2021;118:1-12.
- Lin X, Fu B, Yin S, et al. ORF8 contributes to cytokine storm during SARS-CoV-2 infection by activating IL-17 pathway. *iScience.* 2021;24:102293.
- Geng H, Subramanian S, Wu L, et al. SARS-CoV-2 ORF8 forms intracellular aggregates and inhibits IFNgamma-induced antiviral gene expression in human lung epithelial cells. *Front Immunol.* 2021;12:679482.
- Rashid F, Suleman M, Shah A, et al. Mutations in SARS-CoV-2 ORF8 altered the bonding network with interferon regulatory factor 3 to evade host immune system. *Front Microbiol.* 2021;12:703145.
- Rashid F, Dzakah EE, Wang H, Tang S. The ORF8 protein of SARS-CoV-2 induced endoplasmic reticulum stress and mediated immune evasion by antagonizing production of interferon beta. *Virus Res.* 2021;296:198350.
- Hachim A, Kaviani N, Cohen CA, et al. ORF8 and ORF3b antibodies are accurate serological markers of early and late SARS-CoV-2 infection. *Nat Immunol.* 2020;21:1293-1301.
- Chen SH, Li D, Xu C. Downregulation of Col1a1 induces differentiation in mouse spermatogonia. *Asian J Androl.* 2012;14:842-849.
- Yang M, Chen S, Huang B, et al. Pathological findings in the testes of COVID-19 patients: clinical implications. *Eur Urol Focus.* 2020;6:1124-1129.
- Ozturk R, Tasova Y, Ayaz A. COVID-19: pathogenesis, genetic polymorphism, clinical features and laboratory findings. *Turk J Med Sci.* 2020;50:638-657.
- Govero J, Esakky P, Scheaffer SM, et al. Zika virus infection damages the testes in mice. *Nature.* 2016;540:438-442.
- Wu H, Shi L, Wang Q, et al. Mumps virus-induced innate immune responses in mouse Sertoli and Leydig cells. *Sci Rep.* 2016;6:19507.
- Wen ZN, Cui SY, Duan L, et al. Semen quality of infertile men carrying hepatitis B virus. *Zhonghua Nan Ke Xue.* 2020;26:59-62.
- Piroozmand A, Mousavi Nasab SD, Erami M, et al. Distribution of human papillomavirus and antisperm antibody in semen and its association with semen parameters among infertile men. *J Reprod Infertil.* 2020;21:183-188.
- Kurscheidt FA, Damke E, Bento JC, et al. Effects of herpes simplex virus infections on seminal parameters in male partners of infertile couples. *Urology.* 2018;113:52-58.
- Levy R, Najjoulah F, Keppi B, et al. Detection of cytomegalovirus in semen from a population of men seeking infertility evaluation. *Fertil Steril.* 1997;68:820-825.
- Holtmann N, Edimiris P, Andree M, et al. Assessment of SARS-CoV-2 in human semen—a cohort study. *Fertil Steril.* 2020;114:233-238.
- Hikmet F, Méar L, Edvinsson Å, Micke P, Uhlén M, Lindskog C. The protein expression profile of ACE2 in human tissues. *Mol Syst Biol.* 2020;16:e9610.

34. Zou X, Chen K, Zou J, Han P, Hao J, Han Z. Single-cell RNA-seq data analysis on the receptor ACE2 expression reveals the potential risk of different human organs vulnerable to 2019-nCoV infection. *Front Med*. 2020;14:185-192.
35. Guo L, Zhao S, Li W, et al. Absence of SARS-CoV-2 in semen of a COVID-19 patient cohort. *Andrology*. 2021;9:42-47.
36. Paoli D, Pallotti F, Colangelo S, et al. Study of SARS-CoV-2 in semen and urine samples of a volunteer with positive naso-pharyngeal swab. *J Endocrinol Invest*. 2020;43:1819-1822.
37. Song C, Wang Y, Li W, et al. Absence of 2019 novel coronavirus in semen and testes of COVID-19 patients. *Biol Reprod*. 2020;103:4-6.
38. Baum CL, Arpey CJ. Normal cutaneous wound healing: clinical correlation with cellular and molecular events. *Dermatol Surg*. 2005;31:674-686. Discussion 686.
39. Jin YY, Lin H, Cao L, et al. A convenient and biosafe replicon with accessory genes of SARS-CoV-2 and its potential application in antiviral drug discovery. *Virology*. 2021;36:913-923.
40. Pan JA, Ullman E, Dou Z, Zong WX. Inhibition of protein degradation induces apoptosis through a microtubule-associated protein 1 light chain 3-mediated activation of caspase-8 at intracellular membranes. *Mol Cell Biol*. 2011;31:3158-3170.
41. Pan JA, Sun Y, Jiang YP, et al. TRIM21 ubiquitylates SQSTM1/p62 and suppresses protein sequestration to regulate redox homeostasis. *Mol Cell*. 2016;61:720-733.
42. Chen YQ, Wohlbold TJ, Zheng NY, et al. Influenza infection in humans induces broadly cross-reactive and protective neuraminidase-reactive antibodies. *Cell*. 2018;173:417-429.

SUPPORTING INFORMATION

Additional supporting information can be found online in the Supporting Information section at the end of this article.

How to cite this article: Yu T, Ling Q, Xu M, et al. ORF8 protein of SARS-CoV-2 reduces male fertility in mice. *J Med Virol*. 2022;94:4193-4205. doi:10.1002/jmv.27855